Kalman filter based robust GNSS signal tracking algorithm in presence of ionospheric scintillations

Christophe Macabiau, Lina Deambrogio, Valentin Barreau, Willy Vigneau, Jean-Jacques Valette, Géraldine Artaud, Paul Thevenon, Lionel Ries

Kalman Filter Based Robust GNSS Signal Tracking Algorithm in Presence of Ionospheric Scintillations

Christophe MACABIAU, Lina DEAMBROGIO, *ENAC/Université de Toulouse, Toulouse, France*
Valentin BARREAU, Willy VIGNEAU, *M3SYSTEMS, Toulouse, France*
Jean-Jacques VALETTE, *CLS, Toulouse, France*
Géraldine ARTAUD, Paul THEVENON, Lionel RIES, *CNES, Toulouse, France*

BIOGRAPHY

Christophe MACABIAU graduated as an electronics engineer in 1992 from the ENAC in Toulouse, France. Since 1994, he has been working on the application of satellite navigation techniques to civil aviation. He received his Ph.D in 1997 and has been in charge of the signal processing lab of ENAC from 2000 to 2012. He is currently the head of the TELECOM lab of ENAC.

Lina DEAMBROGIO received the master degree in Telecommunication Engineering in 2007 and the PhD in 2012 both from the University of Bologna, Italy.
From March 2012 she is a Research Fellow in the signal processing lab of ENAC in Toulouse, France.

Willy VIGNEAU is head of the Radionavigation Unit at M3 Systems. Graduated as a Telecommunication Engineer from SUPAERO (Ecole Nationale Supérieure de l'Aéronautique et de l'Espace), he joined M3 Systems in 1999, a French SME (Toulouse) involved in various Radionavigation projects: GPS/EGNOS/Galileo signal processing and critical applications of satellite Radionavigation.

Valentin BARREAU received his electronical engineering degree from ENAC in Toulouse. To validate his degree, he has been doing an internship on GPS occultations at UNB in Canada. He then was working as an engineer at the ISAE, Toulouse. The topic of research was weak GPS signals tracking. Starting September 2010 he joined the M3Systems company to work on GNSS software developments. His main activity relates to multi-sensor hybridization techniques for navigation.

Jean-Jacques VALETTE obtained a PhD thesis in 1992 at Groupe de Recherche de Géodésie Spatiale, University Paul Sabatier of Toulouse, on Geophysics and Space Technics. He has been working at CLS as an engineer in the Metrology of Space Systems Departement and since 2009 in the System and Radio-Frequency Engineering Department. He has been involved in space geodesy for high precision ground positioning projects or the Earth Reference System (DORIS, GNSS). He has been responsible for various space weather studies since 2003 on the fields of ionosphere scintillations, solar energetic particles and on the implementation of operational services.

Géraldine ARTAUD has been a navigation engineer in the CNES Signal and Radionavigation/radiolocalization equipments (SR) department since 2007. She is involved in activities related to GNSS signal analysis, software receivers and simulations.

Paul THEVENON graduated as electronic engineer from Ecole Centrale de Lille in 2004 and obtained a research master at ISAE in space telecommunications in 2007. He obtained a Ph.D. degree in 2010 in the signal processing laboratory of ENAC in Toulouse, France, studying the feasibility of self-positioning a receiver using mobile TV signals is a GNSS. In 2010, he joined the GNSS signal processing team of CNES, the French space research center.

Lionel RIES Lionel RIES is head of the "signal for localisation / navigation" department in CNES, the French Space Agency. The department activities deal with signal design and processing, receivers and payload regarding localisation and navigation systems, including GNSS (Galileo, GNSS space receivers), Search & Rescue by satellite (SARSAT,MEOSAR), and Argos..

ABSTRACT

Ionospheric scintillations are created by diffraction when the transmitted propagating waves encounter a medium made of irregular structures with variable refraction indexes. The recombination of the waves after propagation can be constructive or destructive and the resulting signal at output of the receiver antenna may present rapid variations of phase and amplitude. Scintillations are essentially observed in the regions located under the geomagnetic equator, where irregularities in the ionosphere like plasma bubbles occur

more frequently. They also happen over Polar Regions and are associated with the penetration of charged particles along the magnetic field lines. Under the auroral oval region, scintillations can be local or spread over a great part of the oval. According to past observations scintillations occur mainly at the period of the equinox and the solstice. During the rest of the time there are almost no observations. After sunset, the modification in the ionosphere layers generates such variations. Scintillations cause very brutal and fast fades of the received signal, and once these phenomena occur they can last from 30 minutes up to several hours.

However, continuous GNSS Carrier Phase Measurements are important observations needed for data demodulation and are increasingly used in GNSS receivers, both at user side (e.g. for precise positioning), and for ground segments to compute the navigation and integrity data. The carrier phase is traditionally tracked in the GNSS receivers using PLL, potentially aided by FLL. Carrier tracking loops may be optimized, depending on the application and environment, by selecting the appropriated loop order, integration time, and bandwidth (trade-off between accuracy and robustness).

Phase Loops are however known to be less robust than code tracking loops, and the GNSS receivers may thus suffer from phase tracking loss, for example when tracking low C/N0 signals (attenuations), or fast varying signals such as signals affected by scintillations. This strongly impacts the positioning service availability, as well as the capability to demodulate the navigation message data, in situations where ionospheric scintillations affect the received signal.

One thus has to implement innovative techniques and receiver architectures to provide robust carrier phase tracking, either by improving or optimizing the classical tracking loops (optimized parameters of the PLL, potentially dynamically) or by defining different architectures such as Kalman filter-based tracking loops (either scalar or vector architectures, taking benefits of the different tracking channels, constellations and frequencies which may be differently affected by the disturbance). Other techniques coming, for example, from the telecommunication domain can also be interesting to estimate the propagation channel parameters. It can also be taken advantage of the improved structure of the modern GNSS signals, providing in particular a pilot signal component.

The improvement technique investigated in this paper consists in replacing the conventional phase lock loop filter by a Kalman Filter PLL (KFP), as inspired by the technique proposed by Psiaki et al.. Kalman loop filters provide the optimal filter gain when the statistical levels of uncertainty of the state and observation vectors are well known. So the Kalman filter is continuously adapting the filter bandwidth to the noise level. KFP tracking loop indeed show a better resistance to weak GNSS signal tracking compared to classical loop filters. We were therefore interested in analyzing the potential of such KFP variants for tracking the GPS L1 carrier phase in presence of scintillations, adapting in particular the feedback control signal. This was conducted during a project financed by CNES.

The aim of this paper is therefore to present the development of a GPS L1 phase tracking technique based on a Kalman Filter improving the tracking robustness in presence of ionospheric scintillations, and to present results of its performance using simulations.

The paper starts with a description of the phenomenon of ionospheric scintillation, including the possible models for signals affected by ionospheric scintillations, focusing on the model selected for this study which is GISM (Global Ionospheric Scintillation Model) developed by IEEA. The second section presents a review of the state of the art of ionospheric mitigation tracking techniques. In a third part, the proposed robust GPS L1 tracking technique proposed is described. Then the simulation environment is described, and simulations results are presented, showing improved performance of the proposed tracking technique.

INTRODUCTION

I. BACKGROUND AND SIGNAL MODEL

Scintillation is a well-known phenomenon when observing stars in a summer night, imaging amplitude and phase fluctuations of electromagnetic waves. The cause can be a diffraction when the waves cross a medium composed of irregular structures with variable refraction indexes. An incident plane wave with a uniform phase gets out the medium with a phase which is no longer uniform in space. The recombination of the resulting fields after propagation can be constructive or destructive and can therefore increase or decrease the wave intensity level. This is illustrated in figure 1. The cause can also be a refraction effect when a wave crosses a medium with a phase velocity larger or lower. The wave keeps its plane structure but the signal phase will be the integration of the phase shifts encountered.

Ionospheric scintillations concern signal fluctuations in VHF and UHF radio band up to C band which propagate through the ionized atmospheric layer between 100 and 1000 km, but most particularly in the F2 layer between 250 and 600 km, when it is affected by heterogeneities. The intensity of the effects depends on the signal frequency compared to the plasma frequency and the level of irregularity. In the L band, GNSS is therefore affected too.

Several studies showed some effects mainly located along the magnetic equator and at high latitudes in the auroral oval (area of convergence of the Earth magnetic field lines) and in the Polar Cap. These studies also showed a dependency with the solar cycle, as the maximum observed intensities coincide with the maximum UV

radiated by the sun and the maximum electronic density in the ionosphere [BISHOP et al., 1996].

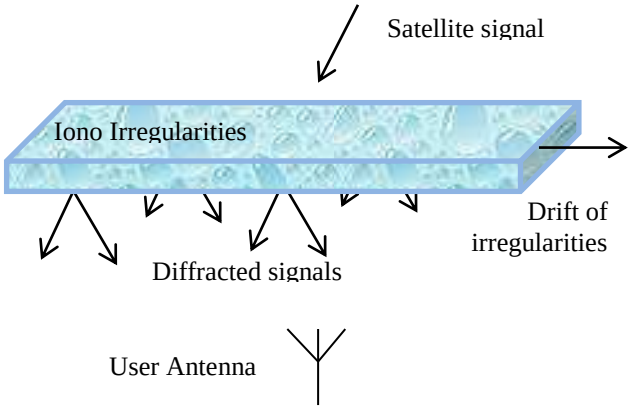

Figure 1: Illustration of diffraction effect from moving ionospheric irregularities leading to ionospheric scintilliation

The physical phenomena that lead to scintillation effects are not well understood yet and are the subject of researches. It is however established that the mechanisms that intervene in the polar region and in the equatorial region have a different nature.

A. Equatorial scintillations

In the case of the equatorial ionosphere, it is largely admitted that the instability mechanism of Rayleigh-Taylor is the main cause of the ionization irregularities that develop after the sunset. In its most frequent form, this phenomenon corresponds to the situation encountered when two non-miscible liquids are in contact, the densest liquid being above the least dense liquid. The equilibrium between the two liquids is unstable and any perturbation causes the least dense liquid to go up and reach the surface. Then, at the interface between the two liquids, some bubbles appear that draw the least dense liquid upwards. In the ionospheric plasma, such bubbles with weak ionization level appear frequently after sunset in the lower part of the ionosphere (typically at altitudes between 200 and 400 km) then go up at higher altitudes and take aigrettes shapes [LASSUDRIE DUCHESNE et al., 2010].
Equatorial scintillations exhibit seasonal variations that superimpose to the modulation of the effects with the position in the solar cycle. Observations in America, Africa and India show the occurrence of peaks at the equinoxes and the quasi total absence of scintillations during summer. In the Pacific, the seasonal influence is inversed with observed maximums from April to August [DOHERTY et al., 2000].

B. High latitude Scintillations

Scintillations at high latitudes are associated with large spatial extension plasmas typically of the order of 100-1000 km in the F region. They are more intense in winter when the solar radiations do not smooth the ionization irregularities.
For the high latitudes, we distinguish the region of the polar cornet in which the magnetic field lines are open to the solar wind and the auroral oval, band centered on the geomagnetic pole between 60 and 75 degrees of latitude. The auroral oval is the area of concentration of shining auroras, emissions linked to particles precipitations coming from the equatorial plasma leaflet, region of the queue of the magnetosphere and carried by aligned electric currents. The oval is run by electric currents (electrojets) that move towards the west. The electrons precipitations happen at an altitude of about 100 km, mainly on the night side along the field lines during sub-storms,sporadic phenomena of a few hours whose origin is in the magnetosphere or during intense solar eruptions ejecting very energetic charged particles (CME : Coronal Mass Ejection). In case of a magnetic storm (Kp>5), the solar wind puts a pressure on the magnetosphere triggering sub-storms but also by extending the limits of the oval towards the south, explaining why boreal auroras were sighted as far in the South as in French Normandy (oct./nov. 2003).
Practically, the polar cornet is an open magnetic region and phase and amplitude scintillations can be met. The aurora oval is a magnetic region where lines are closed, phase scintillations are predominant.

C. Scintillations at mid-latitudes

After an intense magnetic storm and in particular if its origin is a solar eruption with energetic particles, eg. during coronal mass ejection, the engendered ionospheric perturbation can migrate towards the south.

D. Ionospheric scintillations and effects on GNSS signals

The ionosphere causes a group delay of the modulation and a phase advance. Ionosphere irregularities that cause GNSS scintillations can affect the GNSS signal through refraction and diffraction causing rapid variations of the group delay and phase shift of the carrier [KINTNER et al., 2009] as well as strong amplitude attenuations of the signal.
The received GNSS signal can therefore be modeled as:

$$r(t) = A_0 \delta A c(t-\tau) d(t-\tau) \cos(2\pi f_0 t - \theta - \delta\varphi) + n(t)$$

where

- A_0 nominal amplitude of the signal
- f_0 nominal carrier frequency
- d(t) waveform encoding the navigation message
- c(t) waveform encoding the PRN code
- τ propagation delay
- $\theta=\Phi-2\pi f_0\tau$ received carrier phase delay
- Φ initial phase
- δA Scintillation amplitude
- $\delta\varphi$ Scintillation phase

The combination of these phenomena disturbs the lock on the carrier, generating bit errors, cycle slips and even complete loss of the signal tracking. The consequences on GNSS systems are the loss of continuity of service, degradation of accuracy and loss of integrity.
The attenuation of the received GPS signal power in the equatorial region at the maximum of the solar cycle can exceed 20 dB.

a. Observation parameters

Two indices S4 and σ_φ have been defined to characterize these fluctuations. The S4 index characterizes amplitude fluctuations and the σ_φ index characterizes phase fluctuations.
The S4 index is defined as

$$S_4 = \frac{\sqrt{Var(I)}}{E[I]}$$

with $I = A^2 = [A_0 \delta A]^2$ the normalized standard deviation of the fluctuating received signal level
The σ_φ index is used to characterize phase fluctuations and is computed by a receiver as the standard deviation of the phase tracking error at the output of the Phase Lock Loop (PLL) circuit.
It can be modeled as the square root of the sum of three terms [CONKER et al., 2003]:

$$\sigma_\varphi^2 = \sigma_{\varphi_P}^2 + \sigma_{\varphi_T}^2 + \sigma_{\varphi_{osc}}^2$$

- $\sigma_{\varphi_T}^2$ is the contribution due to thermal noise and can be derived as:

$$\sigma_{\varphi_T}^2 = \frac{B_n\left[1 + \frac{1}{2T_i CNo\left(1 - S_4^2(L1)\right)}\right]}{CNo\left(1 - S_4^2(L1)\right)}$$

Where:

  - B_n is the PLL loop bandwidth
  - T_i is the integration time
  - $S_4 < .707$

- $\sigma_{\varphi_P}^2$ is the phase scintillation variance

$$\sigma_{\varphi_P}^2 \cong 2\int_0^\infty |1 - H(f)|^2 S_{\hat{\phi}}(f) df$$

Where $S_{\hat{\phi}}$ is the Power Spectral Density (PSD) of the phase scintillation and $|1 - H(f)|^2$ is the closed loop transfer function of the PLL that depends on k, the loop order, and f_n, the loop natural frequency.

$$|1 - H(f)|^2 = \frac{f^{2k}}{f^{2k} + f_n^{2k}}$$

Typical values are k = 3 and f_n= 1.91 Hz [BENIGUEL et al., 2004].

- And $\sigma_{\varphi_{osc}}^2$ is the contribution due to the receiver oscillator noise.

These indices can be computed over time, and their estimates are generally based on averages obtained over a few tens of seconds. In order to reflect the effect of the scintillation only, it is usually required to remove low frequency variations due to the change of the distance between the satellite and the receiver and local oscillator impact.
Some specific GPS receivers called Ionospheric Scintillation Monitors (ISM) have been developed to remain locked and provide continuous estimates of S_4 and σ_φ, typically every minute.

The physical phenomena generating phase and amplitude scintillations of radio electrical signals are not well known in particular because of a lack of systems and dedicated observation networks that appeared only recently. Existing prediction models only give a global or climatologic representation. They are tuned on observations at different periods of the solar cycle and do not allow short term prediction. They are also limited to equatorial scintillations.

b. GISM

The GISM model (Global Ionospheric Scintillation Model) enables to compute the scintillation effects on a signal after the crossing of the ionosphere between a fixed terrestrial receiver and a GPS satellite. It is a climatological model, statistical properties are associated to the medium to take into account in particular the known characteristics of its spectrum, the effect of the solar cycle and of local time. It uses the MPS technique (Multiple Phase Screen) to solve the wave propagation equations and to determine the expected fluctuations. The medium is divided in successive layers, each acting as a phase screen. The line of sight is first computed considering the different indices of the layers crossed and thus the incident and refracted angles, the electron density is given by the model at each layer by the NeQuick model [RADICELLA, 2009]. The fluctuations and the generated errors are computed by solving the Haselgrove equations. The signal spectrum is characterized by 3 parameters: the slope, the cut-off frequency and the lowest frequency. The slope is comprised between -2 and -3 with -2 as the default value. A detailed model is given in [BENIGUEL, 2010].
The model inputs are:

- The date of the simulations
- The solar flux
- The geographical coordinates at the observation point

The main outputs of the model are:

- The time series of the amplitude and phase of the signals at the selected frequency.
- The estimated S4 and sigma-phi computed every minute.

c. WBMOD

WBMOD is a model developed by NWRA with the support of the US government to estimate a severity level of the effects of the scintillations for a system and of particular environmental conditions. It is a model of the ionosphere that provides the global distribution, a behavior of the electron content irregularities at the origin of scintillations and the system impacts. A scintillation database (Wideband, HiLat and Polar Bear experiences, USAF monitoring network) feeds an empirical model (EDIM) of the irregularities of electron density as the function of date and time, the localization but also the solar activity parameters (number of sunspots) and geomagnetic (Kp). WBMOD allows to estimate the severity of the effects of the scintillations at a given altitude and plots the corresponding map. It does not provide the classical S_4 and σ_φ parameters. It is not adapted for a short term forecast.

Like GISM, WBMOD is also a climatological model but while GISM estimates the classical scintillation parameters and provides time series, WBMOD estimates probabilities that a scintillation level is reached.

d. CSM

CSM (Cornell Scintillation Model) is a model for perturbations of scintillations in amplitude and phase developed by Cornell University. It is only applicable in the equatorial region.

It is a statistical model based on Rice distribution. The disturbed signal component dominated by scintillation uses an autocorrelation function.

The calibration of the model was done with wideband observations at 447 MHz, in UHF and at 1239 MHz. A detailed model is available in [KINTNER et al., 2009]. The model inputs are the S_4 level (with a maximum of 1) and a correlation time called τ_0 (from 0.5 s to 2s for GPS frequency). The model allows for example to generate time series for a GPS SPIRENT signal simulator.

Based on these simulations, performances of robustness of receiver PLL were obtained.

e. Models limitations

The models described above are only applicable in the equatorial region. The phase screen model is insufficient because a distinction is needed between the 2 affected regions, the polar cornet and the auroral oval, each with different mechanisms. Until recently, no prediction model existed for prediction of scintillations for high latitudes. A few recent publications address a tentative of a polar and equatorial model called WAM (Wernick, Alfonsi and Materassi).

For GISM, another limitation of the scintillation model is that it does not reflect reality, which is the presence of low electron density irregularities concentrated in space but a medium with layers with identical characteristics at a given time all around the observation point. Thus, there is no representativity of the fraction of the satellite constellation affected by the phenomenon; all satellites are affected in a homogeneous way.

For Cornell model, its application is also limited to equatorial regions. The other limitations are a maximum value of S_4 of 1 although much higher values can be observed. Also, S_4 and τ_0 are assumed constant during a simulation run, thus generating a stationary pattern. Some authors also consider that this model is susceptible to present biases in GPS frequencies from the fact that some calibration parameters were established in wide band [CIGALA, 2010] .

II. REVIEW OF SCINTILLATION TRACKING TECHNIQUES

In this section, only the techniques at signal processing level will be considered.

The aim of the techniques will thus be to improve the robustness of the carrier phase tracking, in order to increase the capability of the loops to follow accurately the phase variations; the objective will be to decrease the number of phase tracking losses and to limit the impact on the provided measurements (including data demodulation).

This kind of techniques can improve the tracking capability of each signal (receiver channel) without external aiding, or can take benefits of the information coming from other channels tracking (mono- or multi-constellation, on single or dual frequency), or can finally be aided by external sensors information on the receiver dynamic (Doppler aiding by inertial sensors for example).

A. Conventional Loops

Conventional PLL (Phase Lock Loop) are based on close loop filters, which uses discriminator outputs to perform signal tracking. Those conventional architectures have limited performance for tracking phase measurements in difficult conditions, however, smart adaptations of these tracking loops is a good start to achieve good performance in presence of fading, dynamics and scintillations.

Several parameters, such as filter order and loop bandwidth but also the discriminator type, affect the signal tracking behavior of the filter. The higher the order of the filter is, the better the estimation of the residual dynamics will be, but the higher the computational burden will be. Moreover, the loop bandwidth is an important parameter of the loop filter. On one hand, a low loop bandwidth decreases the thermal noise but also slows down the capacity of the filter to follow brutal change of dynamic. On the other hand, a high loop bandwidth increases the thermal noise but the loop filter is able to

follow more precisely the changing of dynamic. The predetection time is another important parameter. It corresponds to the integration time of the signal in the correlators. The longer the signal is integrated, the lower the thermal noise will be. But the dynamic variations have to be followed during the integration process in order not to introduce some dynamic tracking error.

A FLL (Frequency Lock Loop) can also be used and will be more robust than the PLL as it does not control the exact value of the phase of the local carrier, however this loop will not allow the navigation message demodulation. The FPLL (FLL assisted PLL) combines advantages of both PLL and FLL. This loop filter uses two discriminator inputs, one frequency error and one phase error inputs. This loop is more robust than a classical PLL because of the frequency aid. If the phase lock is lost, the FPLL can keep tracking the signal thanks to the frequency aid contrary to the PLL and then restart the phase tracking as soon as the phase is locked again.

All these types of loop are still scalar loops, working in parallel on each channel with a closed-loop filter and having traditionally a constant loop bandwidth. The fine tuning of the loops parameters may increase the robustness of carrier phase tracking but a trade-off is still to be done between accuracy and robustness.

Finally, the closed loops architecture may be improved by reducing the dynamic range of the PLL. This can be done by ultra-tight hybridized receiver architectures, which use some external receiver dynamic information to help the tracking loop filters. By aiding the loop with receiver dynamic information such as speed and acceleration or Doppler, the filter loop bandwidth can be reduced as well as the noise level with an improved robustness to dynamics. However, this solution is limited in case of scintillation because the phase variations (due to scintillation) can be strong and not predicted by external sensors. It will finally be of high interest for high dynamics applications.

B. Adaptive Bandwidth Loops

On top of the classical loops, "Fast Adaptive Bandwidth" (FAB) technique [LEGRAND, 2002] has been developed to minimize the total tracking error in presence of noise and dynamics. This technique is interesting because it allows the receiver to track the signal with a loop bandwidth adapted to the dynamics and the noise level. In case of signal fading, the C/N0 can be very low and at the same time the phase variations very fast (high dynamic or scintillation). That means that the loop bandwidth should increase because of the high dynamic imposed by the scintillation and also decrease because C/N0 is rather low. Because of that, FAB is not really effective during scintillation or high dynamics operation with low C/N0 [KONDO et al., 2007], which is the case most of the time, although it proposes the optimal tuning of the loop bandwidth in this kind of situations.

As the loop is characterized by its transfer function, the discriminator output signal can be predicted and analyzed to perform dynamics and noise estimations. Thus, these estimations are used to build an optimization function that will be minimized by an iterative gradient method in order to provide the corresponding optimal loop filter setting.

C. Kalman Filter-Based Tracking Loops

Other improvement techniques will consist in replacing the conventional loop filter by a Kalman loop filter. Kalman loop filter provides in theory the optimal filter gain when the statistical level of noise of the inputs is well known. In such cases the Kalman filter is continuously adapting the filter bandwidth to the noise level. KFP tracking loop indeed showed a better resistance to weak GNSS signal tracking compared to classical loop filters [ZHANG et al., 2010].

Two options can be considered:

- A 3-state (phase error, Doppler frequency, and Doppler frequency rate) 2-equations (prediction and update) Kalman filter is typically used with a constant gain [PSIAKI et al., 2007], [ZHANG et al., 2009]. In this case the loop bandwidth remains constant but the Kalman filter will allow to track at lower C/N0 and to reduce the cycle slips and loss of lock compared to conventional PLL.
- A 5-equations Kalman filter (including the prediction steps) would allow adaptation of the loop bandwidth. However, this requires to estimate the statistical variance of the input model (state noise and observation noise), which is usually difficult to obtain. In addition, a constant-gain Kalman is more stable than a gain-varying Kalman. Indeed, Kalman filtering can only process parameters subject to gaussian noises, so fixing the gain can avoid filter divergences because of non-gaussian noise effects.

[ZHANG et al., 2010] proposes a Kalman filter architecture with Kalman gain adaptation according to the C/N0 level, which limits the drift of the phase error. The adaptive loop bandwidth combines a weighted Kalman gain with a weighted discriminator estimate to handle the difficult scenario when the filter has no loop bandwidth working range because, for example, of scintillation.

D. Vectorized Architectures

The above solutions are all scalar architectures with a filtered feedback. An alternative is the use of vectorized architecture, which merges observations from all the channels to use most of the available useful information while averaging the tracking errors on each channel and to improve robustness of tracking with aid from all the individual channels tracking. They are usually closed loop architectures but with only one global state vector used in

turn to compute the feedback on each channel filter. NCO's control signals on each channel are thus computed from the residuals of position, velocity and clock offset of the receiver instead of using only code and phase discriminator outputs on each channel.
This kind of architecture allows reducing the impact of jamming and interferences, allows tracking at lower C/N0, and offers a greater immunity to receiver's dynamic. Moreover, in case of signal outage on one of the channel, the receiver keeps following signal dynamic and so allows the tracking function to restart as soon as sufficient signal power comes back.
In particular, Vectorized Delay Frequency Lock Loop (VDFLL) uses information of position and speed of the receiver to compute the Doppler frequency and the code phase of each satellite. The pooling of dynamic information of all the tracking channels allows the receiver to keep tracking satellite signals even when perturbations disturb some of the channels. Indeed, it is possible to re-build the Line-Of-Sight (LOS) distance and the Doppler for each satellite from the position and the speed of the receiver, and so to compute values to send to the NCO of each tracking channel.

These vectorized architectures work well as long as a good receiver's position/velocity is estimated. But as soon as the position estimate is wrong, the position error will be introduced in all the tracking channels and eventually could cause the loss of all the channels. Some integrity position monitoring could be realized to ensure the use of good position and velocity information or the use of good pseudorange information.
An alternative, the Vectorized Phase Lock Loop (VPLL) has been described in [ZHODZISHSKY et al., 1998]. The previous concept of vectorized DLL cannot be directly applied to PLL, due to the inherent ambiguity of the carrier phase and its short wavelength. Indeed a direct transformation between the phase error and the estimated position error is much more difficult to find and the effect of atmospheric errors and dynamic would greatly influence the tracking. This technique is efficient in case of short signal blockage. The PLL will continue the tracking as long as there are enough satellites to compute a precise evolution of the receiver coordinates and clock.
The concept has been pushed further in [HENKEL et al., 2008]. The goal here is to merge data for the same satellite but from different frequencies to determine the dynamic of each parameter and then to remove the satellite-related parameters (ionospheric, tropospheric errors, satellite clock). The receiver-related information (position error, receiver clock) are merged and back transformed to a phase variation which is then integrated separately on each channel.
However, for both techniques, the merging of all channel observations also has some drawbacks, since some perturbations on one of the channel may be reported on all the channels. This will possibly lead to receiver instability or loss of lock on all satellites. The use of integrity monitoring can help removing some perturbed signal from the solution.
In addition, the major drawback is the high processing load and the complexity of the receiver. The Kalman filter or the Least Squares estimation technique used by the vector tracking architecture must be iterated on a time scale commensurate with the integrate-and-dump period used by the algorithm (~ 50 Hz) [PETOVELLO, 2009]. [HENKEL et al., 2008] proved that vectorized phase tracking is working, but at least dual frequency signals have to be processed to remove the maximum of perturbation errors (ionosphere, clocks). This technique is thus very constraining.

E. Other techniques

Other techniques can be used, inherit from other domains such as telecommunication.
For example, wavelet de-noising techniques can help to reduce the noise on tracking channels, based on wavelet transform algorithms. Wavelet transform tends to concentrate the signal energy into a relatively small number of large coefficients. On this basis, a method called wavelet shrinkage to use threshold in wavelet domain was proposed, and it was shown to be asymptotically near optimal for a wide range of signals corrupted by additive Gaussian noise [ZHANG, 2000]. It thus can be useful in case of fading or scintillation to better differentiate noise from dynamic residuals. This technique commonly used for video image de-noising, has been adapted to GNSS field, notably for the acquisition process [TIAN et al., 2008] or for precise point positioning to remove residual errors [WANG et al., 2009]. The results shown by this technique are interesting in terms of performance but the processing load and complexity is rather high and real time implementation may be compromised.
The last type of architecture, very different from the others, is the open loop architecture. Actually, open loop estimators are commonly used in telecommunication (cell phones) in deep urban situations, for example to maintain uplink signal power constant. They have the advantages to be more robust than a closed loop filter since the output is not fed back on the entry of the filter (the errors cannot propagate epoch-to-epoch). Such estimators are used with estimation techniques like Maximum Likelihood Estimation (MLE). Another technique is called Maximum A-Posteriori Estimation (MAP), which uses a priori information about the parameter to evaluate.
In the GNSS world, the closed-loop approach has historically been used in GPS receivers [KONDO et al., 2007]. In this type of receivers, acquisition and tracking are separated. Results from acquisition are used to initialize the tracking. The main advantage of the closed-loop sequential processing is to reduce receiver complexity as only three correlators are required to track the signal. An open-loop batch processing technique is

proposed in [VAN GRAAS et al., 2009], which does not separate acquisition and tracking. A batch of GPS signal is processed once and the signal parameters (code phase, Doppler and carrier phase), are estimated independently from one batch to another.
Finally, this technique offers higher receiver sensitivity because higher integration time can be used. Nevertheless, a Doppler and Doppler rate aiding has to be provided to the receiver to allow a longer integration of the signal. It also reduces the frequency search domain. Another advantage is the immediate re-acquisition when a GNSS signal becomes available. Also, this type of open-loop processing can include the joint estimation of the characteristics of the propagation channel, such as the characteristics of the multipath in case of a deep fading scenario, and specialized techniques can be implemented for this. The major drawback is the large complexity of the receiver and the wide frequency search domain in case no Doppler aid is provided.

F. Synthesis

The techniques analyzed in the previous sections allow a better resistance to noise, co-operation of the channels with each other, loop aiding, and loop bandwidth adaptation. Each technique has advantages and drawbacks that must be considered.

III. ANALYZED KF TRACKING TECHNIQUE

The KFP algorithm (Kalman Filter Phase lock loop) is based on the models and assumptions presented in [PSIAKI et al., 2007]. This algorithm enables to implement a carrier tracking loop of order 3.
The signal processed by the receiver is the received GPS L1 C/A signal. The duration of one bit of the navigation message is thus 20 ms. Let us denote t_k the time samples at which the correlator outputs are provided. We define $\Delta t_k = t_{k+1} - t_k$ the duration of the coherent integrations. We define K the number of correlator outputs available within the duration of one bit of the navigation message. We define I_k and Q_k the correlator outputs available at time t_k, i.e. the correlator outputs computed during the interval $t_{k-1} \dots t_k$.
We define ω_{PLLk} the value of the NCO control signal during the interval $t_k \dots t_{k+1}$. The phase of the PLL NCO is computed as $\phi_{PLL}(k+1) = \phi_{PLL}(k) + \Delta t_k \omega_{PLLk}$.

We define $X_k = \begin{bmatrix} \Delta\phi_k \\ \omega_k \\ \alpha_k \end{bmatrix}$ the state vector of the Kalman Filter, with

- $\Delta\phi_k$ the difference between the phase of the incoming carrier and the phase of the local carrier generated by the NCO
- ω_k the difference between the doppler shift of the incoming carrier and the Doppler shift of the local carrier generated by the NCO in rad/s (pulsation)
- α_k the difference between the jerk of the incoming carrier and the jerk of the local carrier generated by the NCO

This algorithm only includes 2 equations of the Kalman Filter among the 5 traditional equations. Indeed, the Kalman gain K is proposed to be fixed, therefore the two covariance equations, during the prediction and during the update, are useless and are not considered. The algorithm also includes an iterative algorithm allowing deciding the value of the bit of the navigation message affecting the correlator outputs I_{k+1} et Q_{k+1} in order to provide the extended arctangent discriminator outputs. The 2 equations of the Kalman Filter to be run every t_{k+1} are:

$$\begin{bmatrix} \Delta\hat{\phi}_{k+1|k} \\ \hat{\omega}_{k+1|k} \\ \hat{\alpha}_{k+1|k} \end{bmatrix} = \begin{bmatrix} 1 & \Delta t_k & 0.5\Delta t_k^2 \\ 0 & 1 & \Delta t_k \\ 0 & 0 & 1 \end{bmatrix} \begin{bmatrix} \Delta\hat{\phi}_{k|k} \\ \hat{\omega}_{k|k} \\ \hat{\alpha}_{k|k} \end{bmatrix} + \begin{bmatrix} -\Delta t_k \\ 0 \\ 0 \end{bmatrix} \omega_{PLLk}$$

$$\begin{bmatrix} \Delta\hat{\phi}_{k+1|k+1} \\ \hat{\omega}_{k+1|k+1} \\ \hat{\alpha}_{k+1|k+1} \end{bmatrix} = \begin{bmatrix} \Delta\hat{\phi}_{k+1|k} \\ \hat{\omega}_{k+1|k} \\ \hat{\alpha}_{k+1|k} \end{bmatrix} + K\left[\nu_{k+1} - 2\pi \times \text{round}\left(\frac{\nu_{k+1}}{2\pi}\right)\right]$$

The authors of [PSIAKI et al., 2007] propose that the Kalman gain K is not updated, but considered fixed and defined such that the matrix $\begin{bmatrix} 1 & \Delta t_k & 0.5\Delta t_k^2 \\ 0 & 1 & \Delta t_k \\ 0 & 0 & 1 \end{bmatrix} - K\begin{bmatrix} 1 & \frac{\Delta t_k}{2} & \frac{\Delta t_k^2}{6} \end{bmatrix}$ has the eigenvector $\begin{bmatrix} e^{-2\pi B_{PLL}\Delta t_k} \\ e^{[-1+i\sqrt{3}]\pi B_{PLL}\Delta t_k} \\ e^{[-1-i\sqrt{3}]\pi B_{PLL}\Delta t_k} \end{bmatrix}$.
We obtain the values of the gain K, as a function of the desired loop bandwidth and integration time:

- For B_{PLL}=2.5 Hz and Δt_k=0.01 ms, $K = \begin{bmatrix} 0.291004 \\ 4.391752 \\ 33.123850 \end{bmatrix}$
- For B_{PLL}=10 Hz and Δt_k=0.001ms, $K = \begin{bmatrix} 0.121817 \\ 7.533759 \\ 232.944295 \end{bmatrix}$
- For B_{PLL}=10 Hz and Δt_k=0.01ms, $K = \begin{bmatrix} 0.943983 \\ 50.129594 \\ 1323.319695 \end{bmatrix}$
- For B_{PLL}=10 Hz and Δt_k=0.02ms, $K = \begin{bmatrix} 1.475514 \\ 65.065271 \\ 1412.041091 \end{bmatrix}$

The innovation considered is $\nu_{k+1} = y_{k+1} - \hat{y}_{k+1|k}$.
The measurement prediction is:

$$\hat{y}_{k+1|k} = \begin{bmatrix} 1 & \frac{\Delta t_k}{2} & \frac{\Delta t_k^2}{6} \end{bmatrix} \begin{bmatrix} \Delta\hat{\phi}_{k+1|k} \\ \hat{\omega}_{k+1|k} \\ \hat{\alpha}_{k+1|k} \end{bmatrix} - \frac{\Delta t_k}{2}\omega_{PLLk}.$$

The considered measurement vector is computed from the discriminator output. If we want to use an ATAN2 discriminator, it is necessary to estimate the value of the data bit. In this case, the measurement is obtained as $y_{k+1} = \text{atan2}\left(\hat{d}_{bit(k+1|k)} Q_{k+1}, \hat{d}_{bit(k+1|k)} I_{k+1}\right)$.
This discriminator output uses a prediction of the value of the bit of the navigation message under the form:

$$\hat{d}^1_{bit(k+1|k)} = \begin{cases} +1 \text{ si } I_{bit(k+1)}\hat{I}_{bit(k+1|k)} + Q_{bit(k+1)}\hat{Q}_{bit(k+1|k)} \geq 0 \\ -1 \text{ si } I_{bit(k+1)}\hat{I}_{bit(k+1|k)} + Q_{bit(k+1)}\hat{Q}_{bit(k+1|k)} < 0 \end{cases}$$

$$I_{bit(k+1)} = \sum_{i=K\text{floor}\left(\frac{(k+1)}{K}\right)}^{(k+1)} I_i,$$

$$Q_{bit(k+1)} = \sum_{i=K\text{floor}\left(\frac{(k+1)}{K}\right)}^{(k+1)} Q_i$$

And $\hat{I}_{bit(k+1|k)} = \sum_{i=K\text{floor}\left(\frac{(k+1)}{K}\right)}^{(k+1)} \cos\left(\hat{y}_{i|i-1}\right)$,

$\hat{Q}_{bit(k+1|k)} = -\sum_{i=K\text{floor}\left(\frac{(k+1)}{K}\right)}^{(k+1)} \sin\left(\hat{y}_{i|i-1}\right)$

With $\hat{y}_{i|i-1} = \begin{bmatrix} 1 & \frac{\Delta t_{i-1}}{2} & \frac{\Delta t_{i-1}^2}{6} \end{bmatrix} \begin{bmatrix} \Delta\hat{\phi}_{i|i-1} \\ \hat{\omega}_{i|i-1} \\ \hat{\alpha}_{i|i-1} \end{bmatrix} - \frac{\Delta t_{i-1}}{2}\omega_{PLL(i-1)}$

Note that we can envisage another technique of prediction of the navigation message bits which is:

$$\hat{d}^2_{bit(k+1|k)} = \begin{cases} +1 \text{ si } \sum_{i=K\text{floor}\left(\frac{(k+1)}{K}\right)}^{(k+1)} \left[I_i \cos\left(\hat{y}_{i|i-1}\right) - Q_i \sin\left(\hat{y}_{i|i-1}\right)\right] \geq 0 \\ -1 \text{ si } \sum_{i=K\text{floor}\left(\frac{(k+1)}{K}\right)}^{(k+1)} \left[I_i \cos\left(\hat{y}_{i|i-1}\right) - Q_i \sin\left(\hat{y}_{i|i-1}\right)\right] < 0 \end{cases}$$

If the measurement uses the output of an atan discriminator, the estimation of the data bit is then useless and the measurement is directly $y_{k+1} = \text{atan}\left(\frac{Q_{k+1}}{I_{k+1}}\right)$.
Note that the authors of [PSIAKI et al., 2007] propose to compute the NCO control signal ω_{PLLk} in the following way:

$$\omega^1_{PLL(k+1)} = \frac{1}{\Delta t_{k+1}}\left[(1-\eta)^2\left(\Delta\hat{\phi}_{k|k} - \Delta\phi_{des}\right) + (1-2\eta)\Delta t_k\left(\hat{\omega}_{k|k} - \omega_{PLLk}\right) - \eta\Delta t_k^2\hat{\alpha}_{k|k}\right] + \hat{\omega}_{k|k} + \frac{(\Delta t_k + \Delta t_{k+1})^2}{2\Delta t_{k+1}}\hat{\alpha}_{k|k}$$

Where:

- $\Delta\phi_{des}$ is such as $\Delta\hat{\phi}_{k+2|k+2} - 2\,\eta\Delta\hat{\phi}_{k+1|k+1} + \eta^2\Delta\hat{\phi}_{k|k} = (1-\eta)^2\Delta\phi_{des}$
- η is a tuning factor that can be chosen such as $\eta = 0.774597$, or very close to 1 if we want to limit the velocity of convergence of $\Delta\phi_k$ towards $\Delta\phi_{des}$

Another simpler feedback can also be used. This feedback does not use the parameter « etha » which enables to smooth the rapid variations of the phase:

$$\omega^2_{PLL(k+1)} = \frac{1}{\Delta t_{k+1}}\Delta\hat{\phi}_{k|k} + \hat{\omega}_{k|k} + \frac{\Delta t_{k+1}}{2}.\hat{\alpha}_{k|k}$$

In the static case, the smoothing feedback using $\omega^1_{PLL(k+1)}$ is used. This feedback depends on « etha » a smoothing parameter which enables to limit the reactivity of the feedback and thus stabilizes the loop filter. The tracking configuration of the improved receiver is presented in table 1.

	Nominal Scintillations	**Intense Scintillations**	**Worst case Scintillations**
Discri	atan2 + known nav bits	atan2 + known nav bits	atan2 + known nav bits
Bl (Hz)	10	10	3
Integration time (ms)	10	10	1
Etha (η)	0.77	0.77	0.96

Table 1: Tracking configurations of improved receiver adopted for scintillation in the static case

In the dynamic case, the feedback $\omega^2_{PLL(k+1)}$ is used. Contrary to the static case, parameter « etha » is not used, because the dynamics of the receiver is too difficult to follow. This feedback allows a faster reaction to the strong variations of the control signal contrary to the static case as the smoothing tuned by « etha » is not used.

For nominal and intense scintillations, the discriminator used depends on the estimated value of C/N_0 and on the navigation data bit. Above 35dBHz, atan2 is used but only if the two methods for data bit estimation give the same result. In the contrary, atan is used.

	Nominal Scintillations	**Intense Scintillations**	**Worst case Scintillations**
Discri	atan2 if (C/N_0>35dBHz and $\hat{d}_1 = \hat{d}_2$) atan if	atan2 if (C/N_0>35dBHz and $\hat{d}_1 = \hat{d}_2$) atan if	atan

	C/N_0<35dBHz	C/N_0<35dBHz	
Bl (Hz)	10	10	3
Integration time (ms)	10	10	1
Etha (η)	X	X	X

Table 2: Tracking loop configurations of the improved receiver in the dynamic case

IV. SIMULATIONS DESCRIPTION

This section describes the simulation environment used to model the scintillation phenomena, the GNSS signal processing modules (signal generation and reception architectures) and the classical GNSS signal tracking algorithm.

The simulator selected to run the simulations is the JGNSS simulator, owned by CNES. It models a GPS L1 C/A processing chain including: bit level GPS L1 C/A signal generation, propagation channel model including scintillation and multipath, GPS L1 C/A tracking.
Position calculation module is not run in this study that focuses on the robustness of the tracking loops.
Signal duration of 100 seconds was selected for the simulations. This duration is sufficiently long for the GNSS tracking loops to be disturbed by the scintillations and for the simulation time to remain acceptable (about 12h).

The architecture of the standard receiver is classical. It is based on FLL aided PLLs pushing the DLL using correlator outputs. The correlators and the loops are set with parameters having classical values (Bl=1 Hz for the DLL and Bl=10Hz for the FLL and PLL, Early minus Late chip-spacing =0.25). Integration time of 20 ms is used.
The RF bandwidth will be assumed to be different between the static case (ground station) and dynamic case (aircraft in approach), for the simulations with the standard receiver or for the simulations with the enhanced receiver.

Two cases are considered:

- Static receiver (ground station)
- Dynamic receiver in an aircraft in approach. A straight line descent with a constant velocity of 70 m/s is considered.

As we can see, the improved receiver has improvement features compared to the classical receiver:

- In the static case, the improved receiver uses an atan2 phase discriminator with known data bits and a Kalman filter. The integration time is 10ms for the improved receiver compared to the classical receiver.
- In the dynamic case, the improved receiver uses an atan2 phase discriminator when C/N_0>35dBHz, and a Kalman filter. When the C/N_0 is low, both the classical and the improved receivers use an atan phase discriminator.

	Ground station	Aircraft
Sampling Frequency	100MHz	100MHz
Intermediate frequency Fi	4MHz	4MHz
RF/IF Bandwidth	8 MHz	2 MHz
Number of quantization bits in ADC	3 bits	3 bits

Table 3: Receiver parameters

The multipath model to be considered is described below.

In the static case, because the observation interval signal is lower than the period of repetition of the GPS constellation ground tracks, although the geometry between the ground obstacles and the ground station is fixed, the periodicity of the errors due to multipath is not taken into account.
The model proposed is the combination of two sub-models: the first part is a model of the parameters of the multipath, the second part is a model of the impact of this multipath on the pseudorange measurements.
The model of the parameters of the multipath is simplified mainly by drawing randomly these parameters. We propose to consider simultaneously 2 reflected rays at each epoch.
The 2 reflected rays considered are a ray reflected by the ground underneath the antenna, and a ray reflected by a random obstacle located around the antenna.

In the dynamic case, the high resolution aeronautical model developed for the European Space Agency (ESA) in 2002 by Joanneum Research, University of Vigo and the DLR, based on measurements is used **Erreur ! Source du renvoi introuvable.**.
This model includes a direct (Path 0), a refracted component (Path 1), a strong fuselage echo changing very slowly (Path 2), and a ground echo changing very rapidly (Path3). The outputs of this model are the multipath parameters: relative delay, relative amplitude and relative carrier phase shift.
The values of the parameters of the 3 refracted and diffracted rays can then be used to evaluate the carrier and code tracking errors.
Three scintillation scenarios were selected:

- A nominal scintillation scenario: it occurred on 23/10/2010, with a solar flux of 78, which is rather favorable. The S_4 is set to 0.3.

- An intense scintillation scenario: it occurred on 01/12/2006, with a solar flux of 84. The S_4 is set to 0.5.
- A worst case scintillation scenario: it occurred on october 2003. The solar flux reached a maximum of 279. The S_4 is set to 0.9.

Furthermore, two values of C/N0 will be considered for the undisturbed direct path: a C/N0 of 45dBHz and a C/N0 of 35dBHz.

A. GISM simulated data

GISM was selected for this study since it allows to generated amplitude and phase time series of the signal at antenna output. However, we know that the model is limited to the equatorial region and provides an identical effect for all satellites of the constellation – excepted the geometry effects – because it does not consider the presence of bubbles of electronic plasma.

CLS bought the GISM software from the company IEEA. This software provides the times series of the phase and amplitude fluctuations of the signals with a 50 Hz update rate as well as the scintillations parameters S_4 and sigma-phi for the different scenarios considered.

These samples are interpolated in a linear way to bring them to the simulator sampling frequency of 100MHz.

The following figures illustrate the phase and amplitude variations of the signal for the scintillation scenarios considered.

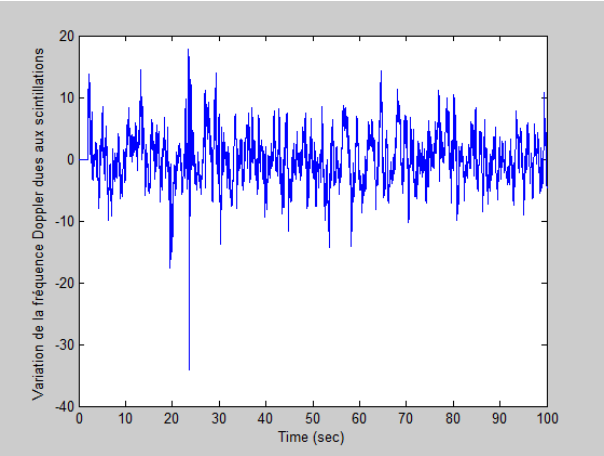

Figure 2: Variations of the received signal Doppler offset in the nominal scintillation case

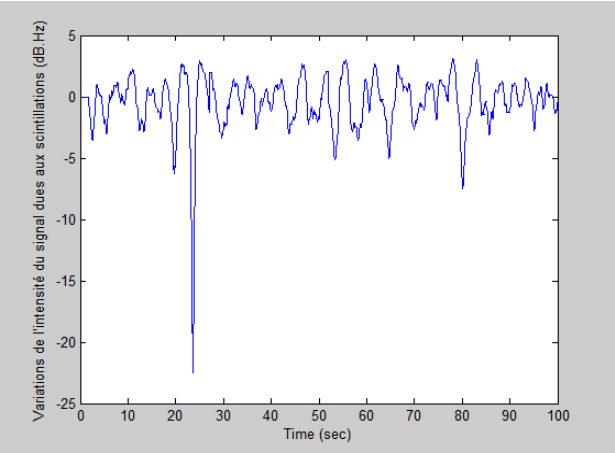

Figure 3: Variations of the received signal power in the nominal scintillation case

It was chosen to consider the maximum intensity periods of the simulated scintillations in the GISM file. This explains the presence of the C/N0 peak at -23dBHz. This peak corresponds to the maximum signal intensity variation for nominal scintillations with a solar flux of 78. It is a singular phenomenon which does not represent the classical phase variations for nominal perturbations.

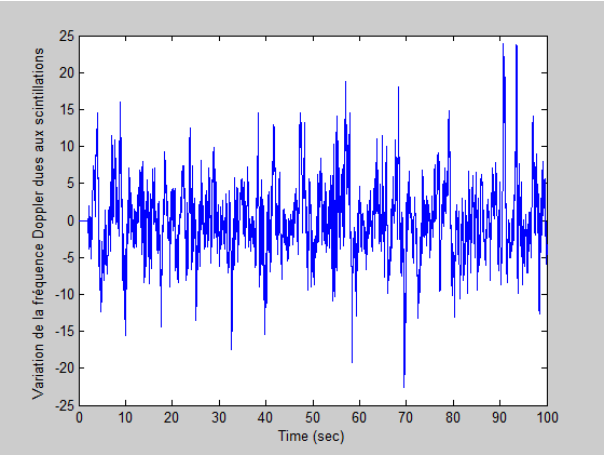

Figure 5: Variations of the received signal Doppler offset in the intense scintillation case

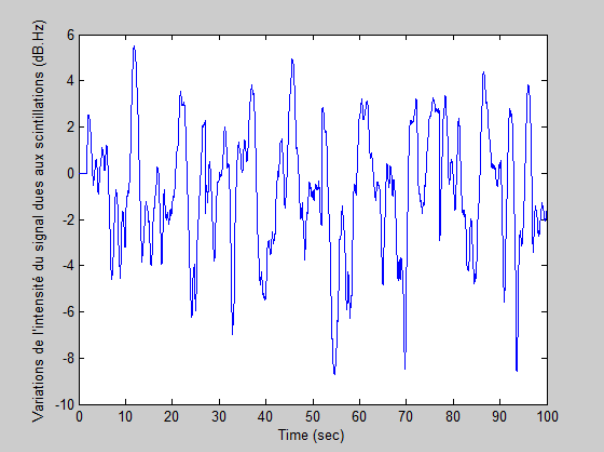

Figure 6: Variations of received signal power in the intense scintillation case

We can see that power variations are larger compared to the normal scintillation case, except for the absence of a very deep C/N0 peak like in the nominal case. These data correspond to a solar flux of 84. We did not choose to consider the maximum case in this situation, so the variations considered are average variations for the intense scintillation case.

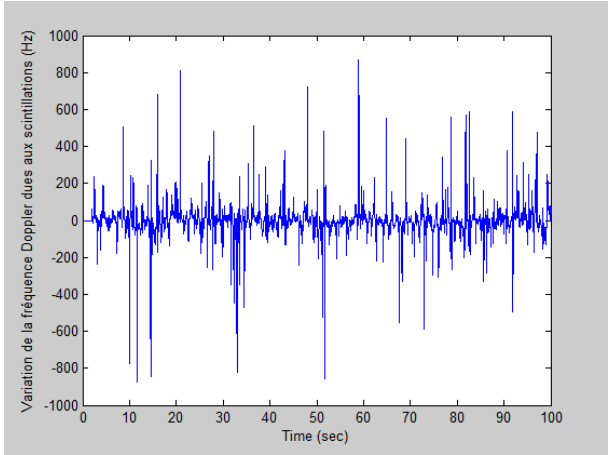

Figure 7: Variations of the received signal Doppler offset in the worst scintillation case

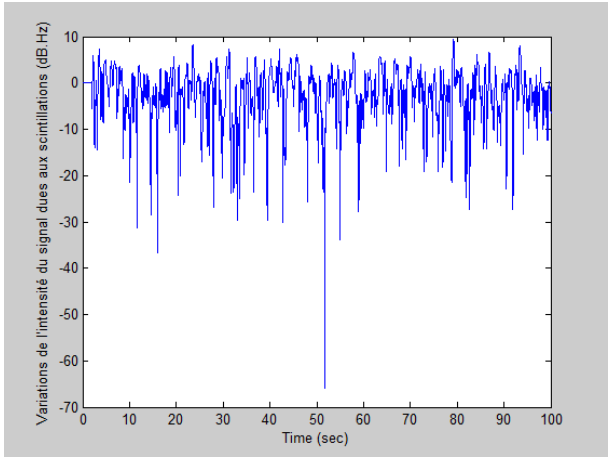

Figure 8: Variations of received signal power in the worst scintillation case

Figure shows the variations of the Doppler offset due to worst case scintillations. We can see that Doppler frequency variations generated by scintillations lie within -800 and +800Hz, meaning that the phase can evolve by 1600*0.02= 32 cycles in 0.02 seconds which is the integration time considered for the standard receiver.
Such a Doppler variation is extreme and results will not be good in such cases.

V. SIMULATIONS RESULTS

We compare here the simulation results obtained with the standard receiver with the results obtained with the improved receiver in the static and dynamic cases.

The table below presents the performance obtained for the static receiver in the standard and improved version (KFP), with the loop filter replaced by a Kalman filter equivalent to a 3rd order filter. Standard and improved receivers are named respectively C and I in the table.
The results obtained are better when a KFP is used than when a FPLL is used.

Sci	C/N0 (dBHz)	Rec	σ_φ (cm)	σ_τ (m)	# of c.s.	# of re-acq	LLR (%)
N	35	I	1.10	2.80	0	1	0.60
		C	1.76	2.72	0	1	1.12
	45	I	0.99	0.89	0	1	0.40
		C	1.37	0.85	0	1	0.51
I	35	I	1.31	2.92	0	1	0.71
		C	1.88	2.55	0	7	3.41
	45	I	1.25	0.99	0	0	0
		C	1.30	0.91	0	6	2.24
W	35	I	673.56	8.63	45	15	44.68
		C	N.A.	N.A.	N.A.	55	49.38
	45	I	693.49	2.33	40	14	37.32
		C	N.A.	N.A.	N.A.	51	39.87

Table 4: Performance obtained for static receiver with KFP and FPLL.

This table 4 presents the better carrier tracking performance of the KFP compared to conventional tracking. In the nominal scintillation scenario, at 35dBHz, the standard deviation of the phase tracking error is 1.10cm for the KFP while it is 1.76cm for the FPLL. At 45dBHz, this sigma is 1cm for KFP while it is 1.37cm for FPLL.
In the worst scintillation case, tracking with the FPLL leads to too many reacquisitions over the 100s simulation time to be able to estimate a valid phase tracking error standard deviation.

In this worst case, the use of KFP with a narrow bandwidth (3Hz) and a large etha (0.96) instead of conventional FPLL allowed decreasing the number of re-acquisitions compared to the FPLL case, and a phase tracking error standard deviation could be estimated. However, the large value of these standard deviations at 35 and 45 dBHz show that the phase is not properly tracked.
This tuning has to be adopted because phase variations can reach 1.6 cycle/ms, which is too fast to be followed through 1 ms integration as the discriminator has an operating region of -0.5…+0.5 cycles.

No significant change of the code tracking error is observed if we compare the nominal and intense simulations cases. At 35dBHz, the standard deviation is around 2.8m, and it is 90cm at 45dBHz, whatever the receiver type.
In the worst simulation case, these values of standard deviation increase a lot (2.33m at 45dBHz, 8.63m at 35dBHz for the improved configuration). Indeed, the carrier Doppler and phase being badly followed, correlator outputs are noisier, and all discriminators are affected. Also, as the DLL is pushed by the carrier tracking, the DLL is affected.

The number of re-acquisitions is highly reduced by using the KFP, except in the nominal case where the singular power loss of 23dB cannot be overcome. The loss of lock rate is also improved.

No cycle slip is observed for the nominal and intense cases, whatever the tracking configuration tested. Numerous cycle slips are observed in the worst simulation case but this is due to the large number of reacquisitions.

The table below presents the performance for the dynamic receiver, with the classical loop filter replaced by an equivalent 3rd order Kalman filter. In this situation, both carrier tracking techniques use an atan discriminator at low C/N0, which has the largest influence on the results.

Sci	C/N0 (dB.Hz)	Rec	σ_φ (cm)	σ_τ (m)	# of c.s.	# of re-acq	LLR (%)
N	35	I	0.91	2.99	0	5 (3)	3.05
		C	2.06	2.89	0	6	2.76
	45	I	0.47	0.89	0	1	0.41
		C	1.55	0.89	0	1	0.51
I	35	I	1.21	4.2	0	9 (4)	8.47
		C	2.92	2.49	0	12	9.1
	45	I	0.60	0.95	0	0	0
		C	1.97	0.88	0	6	2.34
W	35	I	813.3	8.56	47	4 (4)	45.2
		C	N.A.	N.A.	N.A.	45 (in 80s)	53.3
	45	I	419.5	3.26	46	9 (7)	27.34
		C	N.A.	N.A.	N.A.	41 (in 80s)	37.37

Table 5: Table of performance obtained with KFP and FPLL

The estimated standard deviations of the phase tracking errors are lower for the KFP than for the FPLL.

A slight increase of the standard deviation of the code tracking error for the KFP is observed if we compare nominal and intense scintillations. This is thought to be due to the large number of re-acquisitions.
In the worst scintillation case, the standard deviation of the phase tracking error is again large, showing that the phase is not tracked accurately.

As for the static case, the number of re-acquisitions is again low compared to the conventional tracking configuration, except for the nominal scintillation case.
It can also be noted that at 35dBHz for the nominal and intense scintillation, even though the number of re-acquisitions is lower when using the KFP, the loss of lock rate did not decrease. This is due to the fact that the receiver takes more time to achieve bit synchronization after a re-acquisition and stays in a DLL + FLL mode.

In the worst scintillation case, the rate of loss of lock at 45dBHz goes from 37% for the classical dynamic receiver to 27% for the improved dynamic receiver.
The receiver dynamics sometimes creates problems for re-acquisitions and can lead to false peak detections, leading in turn to new re-acquisitions until a meaningful peak is found.

CONCLUSION AND FUTURE WORKS

In this study, it was observed that standard tracking was quite robust for nominal scintillations, but often lost lock in more severe situations. We analyzed an improved tracking technique using a Kalman Filter PLL (KFP) algorithm and proposed enhancements to this technique. We observed that the KFP improved carrier tracking in all situations. However, in our tests, KFP did not improve code tracking.

In the future stages of the study, we can propose the following options for further improvement. First of all, it could be tested a way to adapt the loop bandwidth as a function of detected scintillation intensity. Acceleration input could also be used for tracking loops. It could also be analyzed a way to replace the classical DLL by more robust DLL to improve tracking during strong perturbations. Finally, a frequency discriminator could be added as an additional Kalman filter observable input to maintain carrier tracking even if the phase is not tracked.

REFERENCES

[BENIGUEL et al, 2004] Y. BENIGUEL, B. FORTE, S. M. RADICELLA, H. J. STRANGEWAYS, V. E. GHERM, N. N. ZERNOV "Scintillations effects on satellite to Earth links for telecommunication and navigation purposes", ANNALS OF GEOPHYSICS, SUPPLEMENT TO VOL. 47, N. 2/3, 2004.

[BENIGUEL, 2010] Y. BENIGUEL, "GISM User manual", 2010.

[BISHOP et al., 1996] G. BISHOP, S. BASU, K. GROVES, Phillips. "Upcoming Ionospheric Impacts on GPS at Solar Max What Do We Know/What Do We Need?", ION GPS 1996.

[CIGALA, 2010] "Cigala Project, WP200, State of art review", FP7, 18/05/2010

[CONKER et al., 2003] R. S. CONKER, M. B. EL-ARINI, C. J. HEGARTY and T-Y. Hsiao, "Modelling the Effects of Ionospheric Scintillation on GPS/Satellite-Based Augmentation System Availability". Radio Sci., 37, 1, 1001, doi: 10.1029/2000RS002604, 2003.

[DOHERTY et al., 2000] P. DOHERTY, S. DELAY, C. VALLARDES, J. KLOBUCHAR, "Ionospheric Scintillation Effects in the Equatorial and Auroral Regions", ION GNSS 2000, Salt Lake City, Utah, 662–671, 2000.

[HENKEL et al., 2008] P. Henkel, K. Giger and C. Günther, (2008) "Multi-Carrier Vector Phase Locked loop for Robust Carrier Tracking ". In: Proc. of European Navigation Conference (ENC), 2008-25-04, Toulouse, France.

[KINTNER et al., 2009] P. KINTNER, T. HUMPHREYS, J. HINKS, "GNSS and Ionospheric Scintillation: How to survive the next solar maximum", Inside GNSS, July/August 2009.

[KONDO et al, 2007] Kondo, S., T. Ebinuma, N. Kubo, and A. Yasuda, "Evaluation of tracking performance in the presence of ionosphere scintillation on GPS signal in Japan," Proc. ION GNSS, pp.2832-2839, Ft. Worth, TX, Sept. 2007.

[LASSUDRIE DUCHESNE et al., 2010], P. LASSUDRIE DUCHESNE, Y. BÉNIGUEL, A. BOURDILLON, R. FLEURY, J-J. VALETTE, Minh LE HUY, L. TRAN THI, "Les effets de la scintillation ionosphérique sur le GPS", Navigation, july 2010, vol. 58, n° 231, pp. 17-34, 2010.

[LEGRAND, 2002] F. LEGRAND, Thesis (2002): "Modèle de boucle de poursuite de signaux à spectre étalé et méthode d'amélioration de la précision des mesures brutes », 2002.

[PETOVELLO, 2009] M. PETOVELLO, **"**What About Vector Tracking Loops?", INSIDEGNSS, May/June 2009.

[PSIAKI et al., 2007], M. PSIAKI, T. HUMPHREYS, A. CERRUTI, S. POWELL, P. KINTNER, "Tracking L1 C/A and L2C signals through ionospheric scintillations", ION GNSS 2007.

[RADICELLA, 2009] S. RADICELLA, "The NeQuick model genesis, uses and evolution", Annals of Geophysics, vol 52, N° 3-4, 2009.

[STEINGASS et al., 2004] A. STEINGASS, A. LEHNER, F. PEREZ-FONTAN, E. KUBISTA, M. JESUS MARTIN and B. ARBESSER-RASTBURG, "The High Resolution Aeronautical Multipath Navigation Channel", ION GPS 2004.

[TIAN et al., 2008] J. TIAN, L. YANG, B. HANG, "A Novel GNSS Weak Signal Acquisition Using Wavelet Denoising Method", Proceedings of the 2008 National Technical Meeting of the Institute of Navigation January 28 - 30, 2008.

[VAN GRAAS et al., 2009] F. VAN GRAAS, A. SOLOVIEV, M. U. de HAAG, and S. GUNAWARDENA, "Closed-Loop Sequential Signal Processing and Open-Loop Batch Processing Approaches for GNSS Receiver Design", IEEE Journal of Selected Topics in Signal Processing, Vol. 3, No. 4, 2009.

[WANG et al., 2009] J. WANG, J. WANG, C. ROBERTS, School of Surveying and SIS, UNSW, "Reducing Carrier Phase Errors with EMD Wavelet for Precise GPS Positioning", Survey Review, 41 (312), pp. 152–161, 2009.

[ZHANG et al., 2000] JQ. ZHANG, ZM. GAO, DF. GUO, "Application of Wavelet De-noising to Spectrum-Coding Transmission", Acta Electronica Sinica, Vol 10, 2000.

[ZHANG et al., 2009] L. ZHANG, Y. MORTON, "Tracking GPS Signals under Ionosphere Scintillation Conditions", ION GNSS 2009.

[ZHANG et al., 2010] L. ZHANG, Y. MORTON, F. VAN GRAAS, T. BEACH, "Characterization of GNSS signal parameters under ionosphere scintillation conditions using software based tracking algorithms," Proc. ION/IEEE PLANS 2010, Indian Wells/Palm Springs, CA, May. 2010.

[ZHODZISHSKY et al., 1998] M. ZHODZISHSKY, S. YUDANOV, V. VEITSEL, J. ASHJAEE, "Co-OP Tracking for Carrier Phase," Proceedings of the 11th International Technical Meeting of the Satellite Division of The Institute of Navigation (ION GPS 1998), Nashville, TN, September 1998, pp. 653-664.